

One Model for Two Tasks: Cooperatively Recognizing and Recovering Low-Resolution Scene Text Images by Iterative Mutual Guidance

Minyi Zhao^a, Yang Wang^b, Jihong Guan^b, Shuigeng Zhou^{a,*}

^a*Shanghai Key Lab of Intelligent Information Processing, and School of Computer Science, Fudan University, China*

^b*Department of Computer Science and Technology, Tongji University, China*

Abstract

Scene text recognition (STR) from high-resolution (HR) images has been significantly successful, however text reading on low-resolution (LR) images is still challenging due to insufficient visual information. Therefore, recently many scene text image super-resolution (STISR) models have been proposed to generate super-resolution (SR) images for the LR ones, then STR is done on the SR images, which thus boosts recognition performance. Nevertheless, these methods have two major weaknesses. On the one hand, STISR approaches may generate imperfect or even erroneous SR images, which mislead the subsequent recognition of STR models. On the other hand, as the STISR and STR models are jointly optimized, to pursue high recognition accuracy, the fidelity of SR images may be spoiled. As a result, neither the recognition performance nor the fidelity of STISR models are desirable. Then, can we achieve both high recognition performance and good fidelity? To this end, in this paper we propose a novel method called **IMAGE** (the abbreviation of **I**terative **M**utu**A**I **G**uidanc**E**) to effectively recognize and recover LR scene text images simultaneously. Concretely, IMAGE consists of a specialized STR model for recognition and a tailored STISR model to recover LR images, which are optimized separately. And we develop an iterative mutual guidance mechanism, with which the STR model provides

*Corresponding author

Email addresses: zhaomy20@fudan.edu.cn (Minyi Zhao), tongji_wangyang@tongji.edu.cn (Yang Wang), jhguan@tongji.edu.cn (Jihong Guan), sgzhou@fudan.edu.cn (Shuigeng Zhou)

high-level semantic information as clue to the STISR model for better super-resolution, meanwhile the STISR model offers essential low-level pixel clue to the STR model for more accurate recognition. Extensive experiments on two LR datasets demonstrate the superiority of our method over the existing works on both recognition performance and super-resolution fidelity.

Keywords: Scene text image super-resolution, scene text recognition, super-resolution

1. Introduction

Texts in images offer essential information, which can be extracted and interpreted for many text-based understanding tasks (*e.g.*, text-VQA Singh et al. (2019), Doc-VQA Mathew et al. (2021), and ViteVQA Zhao et al.) and various industrial scenarios (*e.g.*, tag recognition Deng et al. (2023), license-plate recognition Kong et al. (2021), and vehicle identification Yin et al. (2023)). Although scene text recognition (STR) from high-resolution (HR) images has achieved great progress and successfully applied to various scenarios (*e.g.* car plate recognition and bank card recognition) due to a series of advanced scene text recognizers Du et al. (2022) developed via deep learning in recent years, the performance of reading low-resolution (LR) scene text images is still unsatisfactory, due to various image quality degradation like blurry and low-contrast Wang et al. (2020); Ma et al. (2023b).

As shown in Fig. 1, existing approaches to read LR text images can be categorized into two groups. The first group directly recognizes texts from LR images, most early STR works fall into this group. However, as pointed out in Wang et al. (2020); Zhao et al. (2022), due to the lack of sufficient pixel information, they are prone to misread the texts. As a result, the text is incorrectly recognized (see Fig. 1(a)). Another group tries to design a scene text image super-resolution (STISR) Lan et al. (2020b,a); Jiang et al. (2019); Chen et al. (2022); Wang et al. (2020) model to serve as a pre-processing technique to recover the missing details in LR images for boosting text recognition performance as well as the visual quality of the scene texts. More and more recently proposed models follow this line. However, these STISR methods may generate imperfect or even erroneous SR images, which will mislead the subsequent recognition. Besides, in STISR works, as the STISR and STR models are jointly optimized, for pursuing high recognition accuracy, the fidelity of SR images may be degraded. For example, as shown

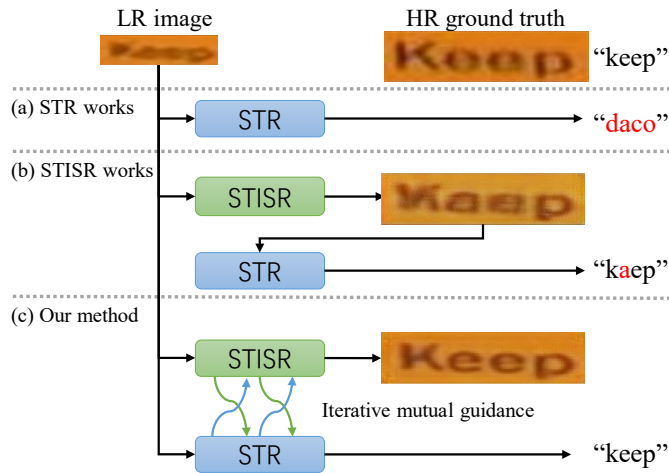


Figure 1: Schematic illustration of existing works: (a) STR methods and (b) STISR methods, and (c) our method IMAGE that employs two models to do recognition and recovery respectively, which are optimized separately, but mutually provide guidance clues to each other in an iterative way. The rightmost character strings are the recognition results, where red characters are incorrectly recognized, and black ones are correctly recognized.

in Fig. 1(b), not only the first ‘e’ is incorrectly recovered, which misleads the subsequent recognition, but also the contrast is enhanced to highlight the texts, which impairs the fidelity of the SR image. As a result, both the recognition performance and the fidelity of STISR models are hurt.

Then, *can we solve the aforementioned problems and achieve win-win in both recognition performance and super-resolution fidelity?* For this purpose, in this paper we propose a new method called **IMAGE** (the abbreviation of **I**terative **M**utu**A**l **G**uidance**E**) to effectively recognize and recover LR scene text images simultaneously, as shown in Fig. 1(c). IMAGE consists of two models: a recognition model to read LR images and a super-resolution model aims at recovering the LR images. The two models are optimized separately to avoid malign competition between them. Meanwhile, we develop an iterative mutual guidance mechanism, with which the STR model provides high-level semantic information as clue to the STISR model for better super-resolution, meanwhile the STISR model offers essential low-level pixel clue to the STR model for more accurate recognition. This mechanism is illustrated by the blue and green curves in Fig. 1(c). The iterative interaction between the recognition model and the STISR model helps them reach their

own goals cooperatively.

Contributions of this paper are as follows:

- Observing the limitations of existing STR and STISR models, we propose a new solution to recognize and recover LR text images simultaneously.
- We develop an iterative mutual guidance mechanism to coordinate the two models so that they are optimized separately, while help each other to reach their own goals by providing informative clues.
- We conduct extensive experiments on two LR datasets, which show the advantages of IMAGE over existing techniques on both recognition performance and super-resolution fidelity.

2. Related work

Here we briefly review the super-resolution techniques and some typical scene text recognizers, and highlight the differences between existing works and our method.

2.1. Scene text image super-resolution

According to whether exploiting text-specific information from HR images, recent STISR methods can be roughly divided into two types: generic super-resolution approaches Ma et al. (2017); Ates et al. (2023) and scene text image super-resolution approaches. Generic image super-resolution methods usually use pixel information captured by pixel loss functions (*i.e.*, L1 or L2 loss) to supervise their models. In particular, SRCNN Dong et al. (2015); Pandey et al. (2018) designs various convolutional neural networks. Xu et al. (2017) and SRResNet Ledig et al. (2017) adopt generative adversarial networks. RCAN Zhang et al. (2018) and SAN Dai et al. (2019) introduce attention mechanisms to advance the recovery. Recently, transformer-structured methods Li et al. (2021); Liang et al. (2021); Wang et al. (2022) are proposed to further boost performance. Differently, STISR approaches focus on extracting various text-specific information to help the model. Specifically, Fang et al. (2021a); Wang et al. (2019); Qin et al. (2022) calculate text-specific losses. Mou et al. (2020) introduces a pluggable super-resolution module. Wang et al. (2020) employs TSRN and gradient profile loss to capture sequential information of text images and gradient fields of

HR images for sharpening the texts. PCAN Zhao et al. (2021) proposes to learn sequence-dependent and high-frequency information for recovery. STT Chen et al. (2021a) uses a pre-trained transformer recognizer for text-focused super-resolution. TG Chen et al. (2022) exploits stroke-level information from HR images for more fine-grained super-resolution. TPGSR Ma et al. (2023a), TATT Ma et al. (2022), C3-STISR Zhao et al. (2022), and Huang et al. (2023) make use of various text-specific clues to guide the super-resolution. Nevertheless, these STISR methods have the drawbacks of forcing STR models to read erroneous SR images and not being able to balance recognition performance and fidelity on SR images. Thereby, both the recognition ability and fidelity are unsatisfactory.

2.2. Scene text recognition

Text recognition on HR images has made great progress in recent years Bai et al. (2018); Chen et al. (2021b,c); Cheng et al. (2017, 2018). Specifically, CRNN Shi et al. (2016) takes CNN and RNN as the encoder and proposes a CTC-based Graves et al. (2006) decoder. ASTER Shi et al. (2018) introduces a spatial transformer network (STN) Jaderberg et al. (2015) to rectify irregular text images. MORAN Luo et al. (2019) proposes a multi-object rectification network. Hu et al. (2020); Sheng et al. (2019); Yu et al. (2020) use different attention mechanisms. AutoSTR Zhang et al. (2020) employs neural architecture search (NAS) Elsken et al. (2019) to search backbone. More recently, semantic-based Qiao et al. (2020); Yu et al. (2020), transformer-based Atienza (2021), linguistical-based Fang et al. (2021b); Wang et al. (2021), and high-efficiency Du et al. (2022); Bautista and Atienza (2022) approaches are proposed to further lift the performance. Although these methods are able to handle irregular, occluded, and incomplete text images, they still have difficulty in recognizing low-resolution images due to the lack of sufficient pixel information. What is more, finetuning these recognizers is insufficient to accurately recognize texts from LR images, as reported in Wang et al. (2020). Therefore, existing STR techniques can not handle text reading of LR images well.

2.3. Differences between related works and our method

First, comparing with recent STR methods, IMAGE not only takes the advantage of pixel information to aid recognition but also outputs an SR image of high fidelity. Second, in contrast to STISR models that require

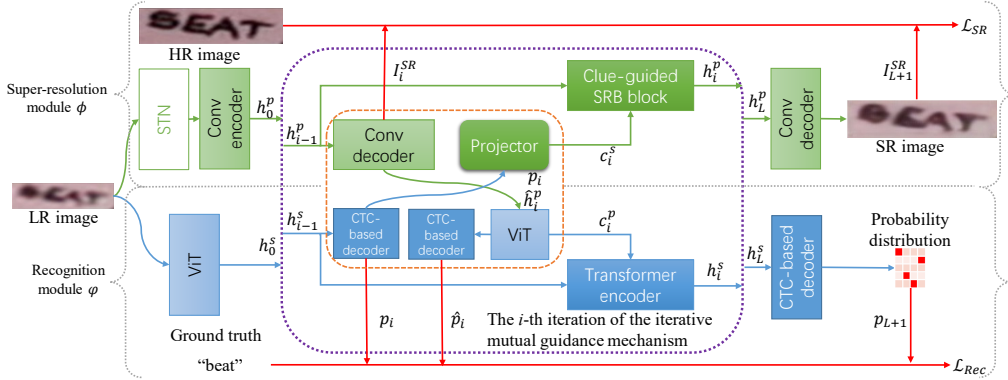


Figure 2: The architecture of our method IMAGE.

STR models to directly read the SR images that may carry noisy or erroneous information, we provide low-level information as indirect clue to aid the recognition. Besides, we relax the requirement of lifting recognition performance on the STISR model so that it can focus on improving fidelity. Our iterative mutual guidance mechanism lets the STISR and STR models help each other cooperatively. As a result, IMAGE outperforms STISR models on both recognition and fidelity.

3. Methodology

Here we first give an overview of our method IMAGE, then present the design of super-resolution model and the text recognition model. Subsequently, we introduce the iterative mutual guidance mechanism in detail, followed by the design of loss function and the overall training procedure to better demonstrate the implementation.

3.1. Overview

Given a low-resolution image $I_{LR} \in \mathbb{R}^{C \times N}$. Here, C is the number of channels of each image, $N = H \times W$ is the collapsed spatial dimension, H and W are the height and width of the LR image. Our aim is to produce a super-resolution (SR) image $I_{SR} \in \mathbb{R}^{C \times (4 \times N)}$ based on the input LR image I_{LR} and recognize the text on I_{LR} .

Fig. 2 shows the architecture of our method IMAGE, which is composed of three major components: the *super-resolution model* ϕ (painted in green)

aims at recovering the LR image, the *recognition model* φ (colored in blue) recognizes the text from the LR image, and an *iterative mutual guidance mechanism* (colored in orange), which is the core component of IMAGE, is used to bridge ϕ and φ and extract useful clues to guide the recognition and recovery. To achieve a more comprehensive interaction, such mechanism is conducted repeatedly over L iterations.

In the i -th iteration, two features from the last iteration are taken as input, namely *pixel feature* $h_{i-1}^p \in \mathbb{R}^{C' \times N}$ where C' is the intermediate channel number, and *semantic feature* $h_{i-1}^s \in \mathbb{R}^{M \times D}$ where M and D denote the number of the tokens and the dimensionality of the tokens, respectively, to produce two clues to aid the corresponding tasks, denoted as *semantic clue* $c_i^s \in \mathbb{R}^{C' \times N}$ for super-resolution and *pixel clue* $c_i^p \in \mathbb{R}^{M \times D}$ for text recognition.

Furthermore, we generate three intermediate results, including an SR image I_i^{SR} , a predicted probability distribution $p_i \in \mathbb{R}^{M \times |\mathcal{A}|}$ of the last semantic feature h_{i-1}^s where $|\mathcal{A}|$ is the size of a charset \mathcal{A} , and a probability distribution $\hat{p}_i \in \mathbb{R}^{M \times |\mathcal{A}|}$ of the pixel clue c_i^p , for the supervision of model training. After generating clues, we combine the clues with the last features (*i.e.*, h_{i-1}^p for ϕ and h_{i-1}^s for φ) to generate the features h_i^p and h_i^s . Eventually, two decoders are stacked to decode the final pixel feature h_L^p and semantic feature h_L^s for the generation of the final SR image I_{L+1}^{SR} and the prediction p_{L+1} .

In IMAGE, a total of $L + 1$ SR images, denoted as $\{I_1^{SR}, \dots, I_{L+1}^{SR}\}$, and $2L + 1$ probability distributions (*i.e.*, $\{p_1, \dots, p_{L+1}\}$ and $\{\hat{p}_1, \dots, \hat{p}_L\}$) are generated. We use the HR image I_{HR} of each training LR image and its text-level annotation p_{CT} , all the generated SR images and predicted probability distributions to evaluate the super-resolution loss \mathcal{L}_{SR} and the recognition loss \mathcal{L}_{Rec} for model training.

3.2. Super-resolution model

Different from the existing STISR models, a semantic clue is additionally input to our super-resolution model ϕ to aid the recovery. Thereby, we design the super-resolution model ϕ in the following way: 1) Begin with a Spatial Transformer Network (STN) to address the pixel-level offsets caused by the manual alignment of LR-HR image pairs Wang et al. (2020); Chen et al. (2021a, 2022); Ma et al. (2023a). 2) A convolution encoder is attached to provide the initial pixel feature h_0^p for super-resolution. 3) L clue-guided SRB blocks Ma et al. (2023a); Zhao et al. (2022), each of which consists of convolution layers and two GRUs to capture sequential information, are

subsequently stacked. For the i -th SRB block, we use the last iteration’s feature h_{i-1}^p and the semantic clue c_i^s to conduct a semantic clue guided super-resolution. Formally, let the i -th SRB block be f_i , we have

$$h_i^p = f_i(h_{i-1}^p, c_i^s). \quad (1)$$

Following Ma et al. (2023a); Zhao et al. (2022), the clue is concatenated with the feature map extracted by the convolution layers of the SRB block at channel dimension. 4) A convolution decoder made up of several convolution layers and a pixel shuffle module is attached at the end of L clue-guided SRB blocks to form the final SR Image I_{L+1}^{SR} .

3.3. Text recognition model

In this section, we introduce the design of the text recognition model φ used in IMAGE. Our recognition model is also different from typical STR models to support the recognition of LR images and is additionally fed in a pixel clue to boost the recognition. Notice that the major challenge of reading LR image texts is the lack of sufficient pixel information. Accordingly, we use transformer-based structure, instead of some convolution and pooling operations used in Shi et al. (2016); Du et al. (2022), to implement the recognizer, which performs better at capturing limited and valuable pixel information thanks to the multi-head self-attention mechanism. In particular, similar to the super-resolution model, we first use a ViT with a patch size of $[H, W//32]$ to offer an initial semantic feature h_0^s . In what follows, L transformer encoders are stacked to fuse the recognition feature and the pixel clue. Taking the i -th iteration for instance, let the $(i-1)$ -th semantic feature, current pixel clue, and the i -th transformer encoder layers be h_{i-1}^s and c_i^p , and g_i , respectively. We compute the i -th recognition feature as follows:

$$h_i^s = g_i([h_{i-1}^s, c_i^p]), \quad (2)$$

where $[\cdot, \cdot]$ denotes the concatenating operation. Finally, a CTC-based decoder is employed to predict the final probability distribution p_{L+1} . After decoding p_{L+1} on the charset \mathcal{A} , the text is obtained.

3.4. Iterative mutual guidance

We have introduced how the super-resolution model ϕ and the recognition model φ are designed to support SR images generation and LR images recognition. In this section, we describe how the iterative mutual guidance

mechanism provides the clues to ϕ and φ . In particular, taking the i -th iteration for example, we denote the i -th mutual guidance as u_i , which generates the semantic clue c_i^s and the pixel clue c_i^p according to two previous features h_{i-1}^p and h_{i-1}^s , and additionally outputs three intermediate results, including an SR image I_i^{SR} and two probability distributions p_i and \hat{p}_i , for better representations of the clues. Formally, we have

$$c_i^s, c_i^p, I_i^{SR}, p_i, \hat{p}_i = u_i(h_{i-1}^p, h_{i-1}^s). \quad (3)$$

Notice that there is a modality gap between h_{i-1}^p and h_{i-1}^s ($H \times W$ for the pixel feature while $M \times |\mathcal{A}|$ for the semantic feature). Hence, some cross-modal processing techniques should be used to convert the modalities. Specifically, as shown in the orange rectangle in Fig. 2, five networks are used: a convolution decoder $q_i^{CD} := \mathbb{R}^{C' \times N} \rightarrow \mathbb{R}^{C \times N}$, a projector $q_i^{OJ} := \mathbb{R}^{M \times |\mathcal{A}|} \rightarrow \mathbb{R}^{C' \times N}$, two CTC-based decoders q_i^{CT1} and q_i^{CT2} ($q_i^{CT1} := \mathbb{R}^{M \times D} \rightarrow \mathbb{R}^{M \times |\mathcal{A}|}$, $q_i^{CT2} := \mathbb{R}^{M \times D} \rightarrow \mathbb{R}^{M \times |\mathcal{A}|}$), and a ViT $q_i^{VT} := \mathbb{R}^{C' \times N} \rightarrow \mathbb{R}^{M \times D}$.

For the generation of semantic clue c_i^s to guide super-resolution model, we first use a CTC-based decoder implemented by a fully connection layer to extract the predicted probability distribution:

$$p_i = q_i^{CT1}(h_{i-1}^s). \quad (4)$$

Then, a projector q_i^{PJ} made up of four transposed convolution layers followed by batch normalization and a bilinear interpolation is used to project the high-level feature into pixel-level:

$$c_i^s = q_i^{PJ}(p_i). \quad (5)$$

The processing of the pixel feature h_{i-1}^p is performed as follows: First, a convolution decoder q_i^{CD} is used to generate the SR image according to the feature h_{i-1}^p :

$$\hat{h}_i^s, I_i^{SR} = q_i^{CD}(h_{i-1}^p), \quad (6)$$

where $\hat{h}_i^s \in \mathbb{R}^{C' \times N}$ is the feature output by the pixel shuffle module in the convolution decoder q_i^{CD} . Then, a ViT with a patch size of $[2 * H, W // 16]$ is used to generate the clue containing richer pixel information for the recognition model:

$$c_i^p = q_i^{VT}(\hat{h}_i^s). \quad (7)$$

Finally, to make the pixel clue much more representative, we explicitly use a CTC-based decoder q_i^{CT2} to offer an intermediate result \hat{p}_i for supervision:

$$\hat{p}_i = q_i^{CT2}(c_i^p). \quad (8)$$

Algorithm 1 The training procedure of IMAGE.

- 1: **Input:** $\phi, \varphi, I_{LR}, I_{HR}, p_{GT}, L$
 - 2: Generate initial h_0^p and h_0^s as described in Sec. 3.2 and Sec. 3.3, respectively
 - 3: **for** i in $[1, \dots, L]$ **do**
 - 4: $c_i^s, c_i^p, I_i^{SR}, p_i, \hat{p}_i = u_i(h_{i-1}^p, h_{i-1}^s)$
 - 5: $h_i^p = f_i(h_{i-1}^p, c_i^s)$
 - 6: $h_i^s = g_i([h_{i-1}^s, c_i^p])$
 - 7: Generate the final output I_{L+1}^{SR} and p_{L+1} according to Sec. 3.2 and Sec. 3.3, respectively
 - 8: Compute the loss \mathcal{L} via Eq. (11)
 - 9: **return** \mathcal{L}
-

3.5. Loss functions

Two losses are computed to supervise the model training. It is worth mentioning that we calculate the losses for all the intermediate results generated in Sec. 3.4 to provide the supervision for the representations of the two clues. The first is super-resolution loss \mathcal{L}_{SR} used for ϕ , which can be calculated via the gradient profile loss \mathcal{L}_{GP} Wang et al. (2020) between HR image I_{HR} and all SR images:

$$\mathcal{L}_{SR} = \sum_i 2^i \mathcal{L}_{GP}(I_i^{SR}, I_{HR}). \quad (9)$$

A weight 2^i is used to make the model to put more emphasis on deeper iterations. Besides, a recognition loss \mathcal{L}_{Rec} is calculated to supervise the recognition module by the CTC loss \mathcal{L}_{CTC} between the ground truth p_{GT} and all the intermediate probability distributions:

$$\mathcal{L}_{Rec} = \sum_i 2^i \mathcal{L}_{CTC}(p_i, p_{GT}) + \sum_i 2^i \mathcal{L}_{CTC}(\hat{p}_i, p_{GT}). \quad (10)$$

The final loss of IMAGE is the combination of the super-resolution loss \mathcal{L}_{SR} and the recognition loss \mathcal{L}_{Rec} :

$$\mathcal{L} = \mathcal{L}_{SR} + \mathcal{L}_{Rec}. \quad (11)$$

3.6. Overall training procedure

Here we describe the overall training procedure of IMAGE to better demonstrate the implementation. As presented in Alg. 1, we first generate the initial pixel feature h_0^p and the initial semantic feature h_0^s . Then, L rounds of iterative mutual guidance (Line 3–Line 6) introduced in Sec. 3.4 are performed to conduct a clue-guided super-resolution and recognition. Subsequently, the last SR image I_{L+1}^{SR} and predicted probability distribution p_{L+1} are generated (Line 7). Finally, the loss of IMAGE is computed to supervise the model training (Line 8).

4. Performance Evaluation

In this section, we first introduce the datasets and metrics used in the experiments and the implementation details. Then, we evaluate IMAGE and compare it with state-of-the-art techniques to show its effectiveness and superiority. Finally, we conduct extensive ablation studies to validate the design of our method.

4.1. Datasets and metrics

Following recent STR and STISR works Shi et al. (2016); Chen et al. (2021a); Ma et al. (2022); Zhao et al. (2022), we use the synthetic datasets to pre-train our model and then finetune the model on the low-resolution datasets. The synthetic datasets include Synth90K Jaderberg et al. (2014) and SynthText Gupta et al. (2016). Two real-world low-resolution datasets are TextZoom and IC15-352. In what follows, we give a brief introduction to the low-resolution datasets used for finetuning and performance evaluation.

The **TextZoom** Wang et al. (2020) dataset consists of 21,740 LR-HR text image pairs collected by lens zooming of the camera in real-world scenarios. The training set has 17,367 pairs, while the test set is divided into three settings based on the camera focal length: easy (1,619 samples), medium (1,411 samples), and hard (1,343 samples).

The **IC15-352** Chen et al. (2022) dataset consists of 352 low-resolution images. This dataset is used to check the generalization power of our model trained on TextZoom when being adapted to other datasets.

There are six metrics used in our paper to evaluate the performance of the model from the aspects of recognition ability, fidelity, and efficiency, accordingly. The first metric is *word-level recognition accuracy* which evaluates the recognition performance of various methods. Following the settings of

ID	Method	Datasets	Recognition accuracy				Fidelity performance		Computational cost	
			Easy	Medium	Hard	Average	PSNR (dB)	SSIM ($\times 10^{-2}$)	FLOPs (G)	Params (M)
1	LR	-	-	-	-	-	20.35	69.61	-	-
2	CRNN	S	37.5%	21.4%	21.1%	27.3%	-	-	0.91	8.36
3	SVTR	S	69.1%	45.6%	34.1%	50.8%	-	-	1.90	22.70
4	CRNN	S+L	58.4%	34.1%	27.6%	41.1%	-	-	0.91	8.36
5	SVTR	S+L	80.0%	59.0%	42.4%	61.7%	-	-	1.90	22.70
6	TG ¹	S+L	61.2%	47.6%	35.5%	48.9%	21.40	74.56	1.82	9.19
7	TPGSR ¹	S+L	63.1%	52.0%	38.6%	51.8%	21.18	77.62	4.75	35.33
8	C3-STISR ¹	S+L	65.2%	53.6%	39.8%	53.7%	21.51	77.21	4.54	58.52
9	TG ²	S+L	76.8%	61.5%	43.3%	61.6%	21.40	74.56	2.81	23.53
10	TPGSR ²	S+L	80.9%	62.8%	46.4%	64.5%	21.18	77.62	5.74	49.67
11	C3-STISR ²	S+L	81.6%	63.8%	46.7%	65.1%	21.51	77.21	5.53	72.86
12	IMAGE-1	S	72.5%	56.1%	41.0%	57.5%	19.52	62.47	1.98	31.84
13	IMAGE-1	S+L	81.8%	68.9%	52.2%	68.6%	21.17	71.16	1.98	31.84
14	IMAGE-2	S	72.7%	59.0%	41.6%	58.7%	19.75	63.16	3.41	56.22
15	IMAGE-2	S+L	83.6%	70.0%	54.8%	70.3%	21.92	74.56	3.41	56.22

Table 1: Performance comparison with various methods on the TextZoom dataset. ‘‘Datasets’’ denotes the datasets used to develop the model. Concretely, ‘S’: synthetic dataset; ‘L’: low-resolution dataset. ¹: CRNN as recognizer. ²: SVTR as recognizer.

previous works Chen et al. (2022); Ma et al. (2023a, 2022); Zhao et al. (2022), we remove punctuation and convert uppercase letters to lowercase letters for calculating recognition accuracy. Besides, we report *Peak Signal-to-Noise Ratio* (PSNR) and *Structure Similarity Index Measure* (SSIM) Wang et al. (2004) as the metrics to measure the fidelity performance. As for efficiency, we calculate the *Floating-point Operations per Second* (FLOPs), the number of parameters (Params) of each model, and the inference time cost (ms) to measure the computational cost.

4.2. Implementation details

All experiments are conducted on 4 NVIDIA RTX 3090 GPUs with 24GB memory. The PyTorch version is 1.10. IMAGE is trained using AdamW optimizer with a learning rate of 0.0001. The batch size is set to 256 for pre-training and 64 for finetuning. The intermediate channel number C' is set to 64. M and D are set to 32 and 196, respectively. Following Du et al. (2022); Shi et al. (2016); Zhao et al. (2022); Chen et al. (2022), we use a charset with a length of 36 (*i.e.*, letters and numbers). To better demonstrate the advantage of our technique over different computational requirements, IMAGE with various iteration numbers are evaluated, denoted as IMAGE- L , *e.g.*, for $L = 2$ we have IMAGE-2.

4.3. Comparing with SOTA approaches

4.3.1. Performance improvement on TextZoom

Here, we evaluate our method on the **TextZoom** dataset. In particular, we compare our method with two recognizers including one typical method widely used by recent STISR methods: CRNN Shi et al. (2016) and one recently proposed state-of-the-art recognizer SVTR Du et al. (2022) and three recent STISR methods including TG Chen et al. (2022), TPGSR Ma et al. (2023a), and C3-STISR Zhao et al. (2022). All the results are presented in Tab. 1.

We start by analyzing the performance of existing STR and STISR methods. From Tab. 1, we can see that (1) Typical STR models cannot do the task of low-resolution scene text image recognition well. As can be checked in the 2nd row and the 3rd row, CRNN and the state-of-the-art recognizer SVTR can only correctly read 27.3% and 50.8% images, respectively. In the rest of this paper, we only discuss two typical and efficient recognizers (*i.e.*, CRNN and SVTR). (2) Finetuning these recognizers still cannot do the work well. For example, after finetuning, the recognition performance of CRNN and SVTR is boosted from 27.3% to 41.1% and 50.8% to 61.7%, respectively (see the 4th row and the 5th row), but it is still poor. (3) Obviously, the STR models can only do recognition, cannot generate SR images. (4) STISR methods are proposed to boost the recognition performance by generating SR images. These methods succeed in lifting the recognition accuracy, for example, TG, TPGSR and C3-STISR boost the accuracy of CRNN from 27.3% to 48.9%, 51.8%, and 53.7%, respectively (see from the 6th row to the 11th row). Nevertheless, STISR approaches also have the risk of misleading the recognition. For instance, as can be seen in the 5th and the 9th rows, the performance of TG+SVTR (61.6%) is inferior to that of finetuning SVTR (61.7%).

Then, we pay attention to the performance of our method IMAGE. To better demonstrate the performance of IMAGE under various computational requirements, two variants are designed, namely IMAGE-1 (the 12th and 13th rows) and IMAGE-2 (the 14th and 15th rows). From the 12th to the 15th rows of Tab. 3, we can see that (1) IMAGE-1 is good enough to outperform state-of-the-arts on recognition accuracy. In particular, IMAGE-1 has an accuracy of 68.6%, which is 1.5% higher than C3-STISR+SVTR (the 11th row). It is worth mentioning that our method is much better at recognizing hard samples. Specifically, the improvements of IMAGE-1 on *Medium* and

	CRNN	SVTR	TPGSR	C3-STISR	IMAGE-1	IMAGE-2
Speed (ms)	3.4	21.5	74.0	41.6	35.5	62.7

Table 2: Running speed (measured on a RTX3090 GPU) comparison. CRNN is used as the recognizer for STISR.

Method	Accuracy	FLOPs (G)	Params (M)
SVTR	66.5%	1.90	22.70
TG	66.4%	2.81	23.53
TPGSR	71.3%	5.74	49.67
C3-STISR	75.0%	5.53	72.86
IMAGE-1	76.7%	1.98	31.84
IMAGE-2	80.7%	3.41	56.22

Table 3: Performance comparison with various state-of-the-art baselines on IC15-352 dataset. The recognizer used for STISR methods is SVTR.

Hard settings (5.1% and 5.5%) are higher than that on *Easy* setting (0.2%). This indicates the strong ability of IMAGE on reading low-resolution scene text images. (2) The best fidelity performance is also obtained by our technique. In particular, IMAGE-2 (the 15th row) lifts the PSNR from 21.51 to 21.92. (3) By taking the computational cost into consideration, the advantage of our method are better demonstrated. Consider that all the methods with FLOPs lower than 2.0G, IMAGE-1 achieves the best recognition accuracy and the second-best fidelity. Our IMAGE-2 obtains both the best recognition accuracy and the best fidelity, while decreases the FLOPs from 5.53G to 3.41G and Params from 72.86M to 56.22M. These results indicate the superiority of IMAGE on recognition accuracy, fidelity performance, and computational cost. We do not present results of IMAGE-3. The reasons are two-fold: (1) this version has a Params of 80.6M, which exceeds the Params of other methods; (2) IMAGE-1 and IMAGE-2 are already good enough to outperform the state-of-the-arts.

We also present the running time measured by an RTX3090 GPU to better demonstrate the advantages of our IMAGE method. Related results are given in Tab. 2. Obviously, our IMAGE-1 runs faster than TPGSR and C3-STISR. Although IMAGE-1 is a bit slower than SVTR, it obtains 6.9% higher accuracy and can output high fidelity SR images.

1							
	c770	c776	c776	c776	c776	c776	c776
2							
	lnpup	language	language	language	language	language	language
3							
	mille	mille	mille	mill0	milk	milk	milk
4							
	bnstatron	instagiak	instagrom	insingram	instagram	instagram	instagram
5							
	tracker	tracker	traceer	traceer	tracker	tracker	tracker
6							
	ireiely	excelicnt	excellont	exceleat	excellent	excellent	excellent
7							
	roge s	rgen	rorsts	rogsts	rogers	rogers	rogers
8							
	ter	and	br	pir	rosy	2010	2018
	LR	TG	TPGSR	C3-STISR	IMAGE-2	HR	GT

Figure 3: Examples of generated images and recognition results. Here, GT is ground truth text. Red/black characters are incorrectly/correctly recognized. Texts below pictures in the LR, TG, TPGSR, C3-STISR and HR columns are recognized by SVTR.

4.3.2. Performance improvement on IC15-352

We also report the performance of typical approaches on the IC15-352 dataset. Since there are not LR-HR image pairs in this dataset, we only report accuracy to evaluate the recognition performance. The experimental results are given in Tab. 3. Some similar conclusions can also be drawn. For example, TG+SVTR also deteriorates the recognition performance. And obviously, the best recognition performance is achieved by our method with a low computational cost.

4.4. Visualization

We have conducted extensive quantitative experiments to show the superiority of IMAGE over existing approaches. Here we conduct a visualization study to better demonstrate the advantage of our method. 8 representative cases are given in Fig. 3. The LR and HR columns indicate the input LR and HR images, and the texts below them are directly recognized by SVTR. We can see that (1) typical recognizers cannot recognize well low-resolution text images (see the 1st and the 2nd cases) while STISR methods and our method can do recognition better. (2) The 3rd - 5th cases show one major weakness of typical STISR methods. Obviously, STISR approaches may generate erroneous results and mislead the subsequent recognition. Taking the 3rd case for instance, TG, TPGSR, and C3-STISR mistakenly recover the last character ‘k’ to ‘e’, ‘e’, and ‘o’, respectively. What is worse, for the 5th case, we would rather drop STISR and directly let the recognizer guess the blurry pixels. Fortunately, our method only implicitly uses the super-resolution results as clues to help recognition, which avoids the explicit propagation of errors. (3) As a result, as can be seen in the 6th and the 7th cases, IMAGE can still correctly read some tough cases where the information from the super-resolution model is insufficient or even erroneous (e.g. the recovery of ‘n’ in the 6th case fails). (4) Another limitation of STISR approaches is that they may hurt the fidelity to make the SR images much more distinguishable. For example, in the 7th case, TPGSR slightly over-lightens the background while C3-STISR deepens the shadow of the text to highlight the text. (5) Finally, as can be seen in the 8th case, in some extremely tough cases where IMAGE fails to capture sufficient information from LR images and clues, the recognition and the recovery will fail.

Method	Metrics		
	Accuracy	PSNR(dB)	FLOPs(G)
IMAGE-2	70.3%	21.92	3.41
Recognition model	65.6%	-	1.23
Super-resolution model	-	21.67	1.17
Without losses of IMAGE	57.5%	21.33	3.41

Table 4: Ablation study on the proposed iterative mutual guidance.

i	Metrics			
	Accuracy		PSNR(dB)	FLOPs
	p_i	\hat{p}_i	I_i^{SR}	(G)
1	57.5%	57.1%	21.13	1.70
2	67.3%	61.4%	21.29	3.14
3	70.3%	-	21.92	3.41

Table 5: Performance of the i -th intermediate results of IMAGE-2.

4.5. Ablation study

Here we conduct an ablation study to check the advantage of IMAGE. We start by develop a variant without iterative mutual guidance, which means the recognition model and the super-resolution model are optimized individually without any interaction. As can be seen in the 2nd and 3rd rows of Tab. 4, all the performances without IMAGE technique are deteriorated and IMAGE uses only an additional cost of 1.01G FLOPs to lift the accuracy from 65.6% to 70.3% and PSNR from 21.67 to 21.92. This shows the effectiveness of the proposed IMAGE. Besides, we also design a variant that removes the losses calculated for the supervision of the clues introduced in Sec. 3.4. We can see in the 4th row of Tab. 4, the performance is significantly degraded. This validates the importance of our loss functions that can make clues much more informative.

Then, we report performance of the intermediate results of IMAGE-2 to better demonstrate the effectiveness of the clues generated by IMAGE. The metrics including the recognition performance of $\{p_i\}_{i=1}^{L+1}$ and $\{\hat{p}_i\}_{i=1}^L$, the fidelity of $\{I_{SR}^i\}_{i=1}^{L+1}$, and the cumulative computational cost. We can see in Tab. 5 that (1) the corresponding performance of the intermediate results is improved step by step with the help of the cross-modal clues. (2) Reading \hat{p}_i that comes from the SR model is inferior to reading p_i that is generated by semantic feature h_{i-1}^s and clue c_{i-1}^p , which means that the SR images usually



Figure 4: Examples of the intermediate recognition results and SR images of IMAGE-2. Here, GT indicates ground truth. Red/black characters indicate incorrectly/correctly recognized.

bring erroneous information and reading the texts with SR features as clue is a better solution. (3) It takes 0.26G FLOPs to offer initial features, 1.44G for each iteration, while 0.27G to decode the final results.

Finally, we also visualize the intermediate results in Fig. 4. As can be seen in Fig. 4, the intermediate results are improved step by step. In particular, in the left case, the character ‘h’ is corrected in the second iteration while two ‘e’s in the right case are also successfully recovered step by step. By taking these intermediate results as clues, the recognition and super-resolution are also lifted iteratively, which leads to more accurate final results.

5. Limitation and future work

The major limitation of IMAGE is that the generated SR images are targeted for fidelity. Thus, the SR images generated by IMAGE will be a bit less distinguishable, compared with typical STISR works (*e.g.* the 7th case in Fig. 3 and a bit lower SSIM). In addition, our method IMAGE has two separate models for STISR and STR, which makes the model a little complex, though it is not quite large. So as a future, we will try to pursue new solutions that do both recognition and recovery via a single model.

6. Conclusion

In this paper, we propose a new method called IMAGE to do low-resolution scene text recognition and recovery in a framework. Different from existing STR and STISR works that directly read texts from LR images or recover blurry pixels to benefit recognition, IMAGE coordinates a text recognition model and a super-resolution model so that they can be optimized separately for their tasks while providing clues for cooperating with each other. IMAGE successfully overcomes the limitations of existing methods. Extensive experiments on two low-resolution scene text datasets validate the superiority of IMAGE over existing techniques on both recognition performance and super-resolution fidelity.

References

- Ates, H.F., Yildirim, S., Gunturk, B.K., 2023. Deep learning-based blind image super-resolution with iterative kernel reconstruction and noise estimation. *Computer Vision and Image Understanding* 233, 103718.
- Atienza, R., 2021. Vision transformer for fast and efficient scene text recognition, in: *International Conference on Document Analysis and Recognition*, Springer. pp. 319–334.
- Bai, F., Cheng, Z., Niu, Y., Pu, S., Zhou, S., 2018. Edit probability for scene text recognition, in: *Proceedings of the IEEE/CVF conference on computer vision and pattern recognition*, pp. 1508–1516.
- Bautista, D., Atienza, R., 2022. Scene text recognition with permuted autoregressive sequence models, in: *Proceedings of the 17th European Conference on Computer Vision (ECCV)*, Springer International Publishing, Cham.
- Chen, J., Li, B., Xue, X., 2021a. Scene text telescope: Text-focused scene image super-resolution, in: *Proceedings of the IEEE/CVF conference on computer vision and pattern recognition*, pp. 12026–12035.
- Chen, J., Yu, H., Ma, J., Guan, M., Xu, X., Wang, X., Qu, S., Li, B., Xue, X., 2021b. Benchmarking chinese text recognition: Datasets, baselines, and an empirical study. *arXiv preprint arXiv:2112.15093* .

- Chen, J., Yu, H., Ma, J., Li, B., Xue, X., 2022. Text gestalt: Stroke-aware scene text image super-resolution, in: Proceedings of the AAAI Conference on Artificial Intelligence, pp. 285–293.
- Chen, X., Jin, L., Zhu, Y., Luo, C., Wang, T., 2021c. Text recognition in the wild: A survey. *ACM Computing Surveys (CSUR)* 54, 1–35.
- Cheng, Z., Bai, F., Xu, Y., Zheng, G., Pu, S., Zhou, S., 2017. Focusing attention: Towards accurate text recognition in natural images, in: Proceedings of the IEEE International Conference on Computer Vision, pp. 5076–5084.
- Cheng, Z., Xu, Y., Bai, F., Niu, Y., Pu, S., Zhou, S., 2018. Aon: Towards arbitrarily-oriented text recognition, in: Proceedings of the IEEE/CVF conference on computer vision and pattern recognition, pp. 5571–5579.
- Dai, T., Cai, J., Zhang, Y., Xia, S.T., Zhang, L., 2019. Second-order attention network for single image super-resolution, in: Proceedings of the IEEE/CVF conference on computer vision and pattern recognition, pp. 11065–11074.
- Deng, X., Chen, X., Cao, D., Ren, K., Sun, P.Z., 2023. An end-to-end tag recognition architecture for industrial meter. *IEEE Transactions on Industrial Informatics* .
- Dong, C., Loy, C.C., He, K., Tang, X., 2015. Image super-resolution using deep convolutional networks. *IEEE transactions on pattern analysis and machine intelligence* 38, 295–307.
- Du, Y., Chen, Z., Jia, C., Yin, X., Zheng, T., Li, C., Du, Y., Jiang, Y.G., 2022. Svtr: Scene text recognition with a single visual model. *arXiv preprint arXiv:2205.00159* .
- Elsken, T., Metzen, J.H., Hutter, F., 2019. Neural architecture search: A survey. *The Journal of Machine Learning Research* 20, 1997–2017.
- Fang, C., Zhu, Y., Liao, L., Ling, X., 2021a. TsrGAN: Real-world text image super-resolution based on adversarial learning and triplet attention. *Neurocomputing* 455, 88–96.

- Fang, S., Xie, H., Wang, Y., Mao, Z., Zhang, Y., 2021b. Read like humans: Autonomous, bidirectional and iterative language modeling for scene text recognition, in: Proceedings of the IEEE/CVF conference on computer vision and pattern recognition, pp. 7098–7107.
- Graves, A., Fernández, S., Gomez, F., Schmidhuber, J., 2006. Connectionist temporal classification: labelling unsegmented sequence data with recurrent neural networks, in: Proceedings of the 23rd international conference on Machine learning, pp. 369–376.
- Gupta, A., Vedaldi, A., Zisserman, A., 2016. Synthetic data for text localisation in natural images, in: Proceedings of the IEEE conference on computer vision and pattern recognition, pp. 2315–2324.
- Hu, W., Cai, X., Hou, J., Yi, S., Lin, Z., 2020. Gtc: Guided training of ctc towards efficient and accurate scene text recognition, in: AAAI, pp. 11005–11012.
- Huang, C., Peng, X., Liu, D., Lu, Y., 2023. Text image super-resolution guided by text structure and embedding priors. *ACM Transactions on Multimedia Computing, Communications and Applications* 19, 1–18.
- Jaderberg, M., Simonyan, K., Vedaldi, A., Zisserman, A., 2014. Synthetic data and artificial neural networks for natural scene text recognition. arXiv preprint arXiv:1406.2227 .
- Jaderberg, M., Simonyan, K., Zisserman, A., et al., 2015. Spatial transformer networks. *Advances in neural information processing systems* 28.
- Jiang, J., Yu, Y., Wang, Z., Tang, S., Hu, R., Ma, J., 2019. Ensemble super-resolution with a reference dataset. *IEEE transactions on cybernetics* 50, 4694–4708.
- Kong, X., Wang, K., Hou, M., Hao, X., Shen, G., Chen, X., Xia, F., 2021. A federated learning-based license plate recognition scheme for 5g-enabled internet of vehicles. *IEEE Transactions on Industrial Informatics* 17, 8523–8530.
- Lan, R., Sun, L., Liu, Z., Lu, H., Pang, C., Luo, X., 2020a. Madnet: a fast and lightweight network for single-image super resolution. *IEEE transactions on cybernetics* 51, 1443–1453.

- Lan, R., Sun, L., Liu, Z., Lu, H., Su, Z., Pang, C., Luo, X., 2020b. Cascading and enhanced residual networks for accurate single-image super-resolution. *IEEE transactions on cybernetics* 51, 115–125.
- Ledig, C., Theis, L., Huszár, F., Caballero, J., Cunningham, A., Acosta, A., Aitken, A., Tejani, A., Totz, J., Wang, Z., et al., 2017. Photo-realistic single image super-resolution using a generative adversarial network, in: *Proceedings of the IEEE/CVF conference on computer vision and pattern recognition*, pp. 4681–4690.
- Li, W., Lu, X., Lu, J., Zhang, X., Jia, J., 2021. On efficient transformer and image pre-training for low-level vision. *arXiv preprint arXiv:2112.10175* .
- Liang, J., Cao, J., Sun, G., Zhang, K., Van Gool, L., Timofte, R., 2021. Swinir: Image restoration using swin transformer, in: *Proceedings of the IEEE/CVF International Conference on Computer Vision*, pp. 1833–1844.
- Luo, C., Jin, L., Sun, Z., 2019. Moran: A multi-object rectified attention network for scene text recognition. *Pattern Recognition* 90, 109–118.
- Ma, C., Yang, C.Y., Yang, X., Yang, M.H., 2017. Learning a no-reference quality metric for single-image super-resolution. *Computer Vision and Image Understanding* 158, 1–16.
- Ma, J., Guo, S., Zhang, L., 2023a. Text prior guided scene text image super-resolution. *IEEE Transactions on Image Processing* .
- Ma, J., Liang, Z., Xiang, W., Yang, X., Zhang, L., 2023b. A benchmark for chinese-english scene text image super-resolution, in: *Proceedings of the IEEE/CVF International Conference on Computer Vision*, pp. 19452–19461.
- Ma, J., Liang, Z., Zhang, L., 2022. A text attention network for spatial deformation robust scene text image super-resolution, in: *Proceedings of the IEEE/CVF conference on computer vision and pattern recognition*, pp. 5911–5920.
- Mathew, M., Karatzas, D., Jawahar, C., 2021. Docvqa: A dataset for vqa on document images, in: *Proceedings of the IEEE/CVF conference on computer vision and pattern recognition*, pp. 2200–2209.

- Mou, Y., Tan, L., Yang, H., Chen, J., Liu, L., Yan, R., Huang, Y., 2020. Plugnet: Degradation aware scene text recognition supervised by a plug-gable super-resolution unit, in: *Computer Vision–ECCV 2020: 16th European Conference, Glasgow, UK, August 23–28, 2020, Proceedings, Part XV 16*, Springer. pp. 158–174.
- Pandey, R.K., Vignesh, K., Ramakrishnan, A., et al., 2018. Binary document image super resolution for improved readability and ocr performance. arXiv preprint arXiv:1812.02475 .
- Qiao, Z., Zhou, Y., Yang, D., Zhou, Y., Wang, W., 2020. Seed: Semantics enhanced encoder-decoder framework for scene text recognition, in: *Proceedings of the IEEE/CVF conference on computer vision and pattern recognition*, pp. 13528–13537.
- Qin, R., Wang, B., Tai, Y.W., 2022. Scene text image super-resolution via content perceptual loss and criss-cross transformer blocks. arXiv preprint arXiv:2210.06924 .
- Sheng, F., Chen, Z., Xu, B., 2019. Nrtr: A no-recurrence sequence-to-sequence model for scene text recognition, in: *2019 International conference on document analysis and recognition (ICDAR)*, IEEE. pp. 781–786.
- Shi, B., Bai, X., Yao, C., 2016. An end-to-end trainable neural network for image-based sequence recognition and its application to scene text recognition. *IEEE transactions on pattern analysis and machine intelligence* 39, 2298–2304.
- Shi, B., Yang, M., Wang, X., Lyu, P., Yao, C., Bai, X., 2018. Aster: An attentional scene text recognizer with flexible rectification. *IEEE transactions on pattern analysis and machine intelligence* 41, 2035–2048.
- Singh, A., Natarajan, V., Shah, M., Jiang, Y., Chen, X., Batra, D., Parikh, D., Rohrbach, M., 2019. Towards vqa models that can read, in: *Proceedings of the IEEE/CVF conference on computer vision and pattern recognition*, pp. 8317–8326.
- Wang, W., Xie, E., Liu, X., Wang, W., Liang, D., Shen, C., Bai, X., 2020. Scene text image super-resolution in the wild, in: *Computer Vision–ECCV 2020: 16th European Conference, Glasgow, UK, August 23–28, 2020, Proceedings, Part X 16*, Springer. pp. 650–666.

- Wang, W., Xie, E., Sun, P., Wang, W., Tian, L., Shen, C., Luo, P., 2019. Textsr: Content-aware text super-resolution guided by recognition. arXiv preprint arXiv:1909.07113 .
- Wang, Y., Xie, H., Fang, S., Wang, J., Zhu, S., Zhang, Y., 2021. From two to one: A new scene text recognizer with visual language modeling network, in: Proceedings of the IEEE International Conference on Computer Vision, pp. 14194–14203.
- Wang, Z., Bovik, A.C., Sheikh, H.R., Simoncelli, E.P., 2004. Image quality assessment: from error visibility to structural similarity. *IEEE transactions on image processing* 13, 600–612.
- Wang, Z., Cun, X., Bao, J., Zhou, W., Liu, J., Li, H., 2022. Uformer: A general u-shaped transformer for image restoration, in: Proceedings of the IEEE/CVF Conference on Computer Vision and Pattern Recognition, pp. 17683–17693.
- Xu, X., Sun, D., Pan, J., Zhang, Y., Pfister, H., Yang, M.H., 2017. Learning to super-resolve blurry face and text images, in: Proceedings of the IEEE international conference on computer vision, pp. 251–260.
- Yin, G., Huang, S., He, T., Xie, J., Yang, D., 2023. Mirrored east: An efficient detector for automatic vehicle identification number detection in the wild. *IEEE Transactions on Industrial Informatics* .
- Yu, D., Li, X., Zhang, C., Liu, T., Han, J., Liu, J., Ding, E., 2020. Towards accurate scene text recognition with semantic reasoning networks, in: Proceedings of the IEEE/CVF conference on computer vision and pattern recognition, pp. 12113–12122.
- Zhang, H., Yao, Q., Yang, M., Xu, Y., Bai, X., 2020. Autostr: efficient backbone search for scene text recognition, in: *Computer Vision–ECCV 2020: 16th European Conference, Glasgow, UK, August 23–28, 2020, Proceedings, Part XXIV* 16, Springer. pp. 751–767.
- Zhang, Y., Li, K., Li, K., Wang, L., Zhong, B., Fu, Y., 2018. Image super-resolution using very deep residual channel attention networks, in: Proceedings of the European conference on computer vision (ECCV), pp. 286–301.

- Zhao, C., Feng, S., Zhao, B.N., Ding, Z., Wu, J., Shen, F., Shen, H.T., 2021. Scene text image super-resolution via parallelly contextual attention network, in: Proceedings of the 29th ACM International Conference on Multimedia, pp. 2908–2917.
- Zhao, M., Li, B., Wang, J., Li, W., Zhou, W., Zhang, L., Xuyang, S., Yu, Z., Yu, X., Li, G., et al., . Towards video text visual question answering: Benchmark and baseline, in: Thirty-sixth Conference on Neural Information Processing Systems Datasets and Benchmarks Track.
- Zhao, M., Wang, M., Bai, F., Li, B., Wang, J., Zhou, S., 2022. C3-stir: Scene text image super-resolution with triple clues, in: International Joint Conference on Artificial Intelligence, pp. 1707–1713.